Earth Surf. Dynam. Discuss., doi:10.5194/esurf-2016-60, 2016
Manuscript under review for journal Earth Surf. Dynam.
Published: 8 December 2016

Earth Surface Dynamics Discussions

The influence of turbulent bursting on sediment resuspension under fluvial unidirectional currents

Sarik Salim[1], Charitha Pattiaratchi[1], Rafael Tinoco[2], Giovanni Coco[3], Yasha Hetzel[1], Sarath Wijeratne[1], Ravindra Jayaratne[4]

[1]School of Civil Environmental and Mining Engineering and UWA Oceans Institute, University of Western Australia, 35 Stirling Highway, Crawley, WA 6009, Australia
[2]Department of Civil and Environmental Engineering, University of Illinois at Urbana-Champaign, Urbana, IL 61801, USA
[3]Faculty of Science, University of Auckland, Auckland 1142, New Zealand
[4]School of Architecture, Computing and Engineering, University of East London, Docklands Campus, 4-6 University Way, London E16 2RD, UK

Correspondence to: Sarik Salim (sarik.salim@research.uwa.edu.au)

Abstract. Laboratory experiments were undertaken in a unidirectional current flume in order to examine the role of turbulence on incipient sediment motion. An acoustic Doppler velocimeter was used to measure the instantaneous three-dimensional velocity components and acoustic backscatter (related to suspended sediment concentration). The relationship between wall turbulence (in particular, the 'bursting' phenomenon) and resuspension of a non-cohesive sediment bed was examined. The results within a range above and below the measured critical velocity suggested that: 1) the contribution of turbulent bursting events remained identical in both experimental conditions; 2) ejection and sweep events contributed more to the total sediment flux than up-acceleration and down-deceleration events; and 3) wavelet transform revealed a correlation between the momentum and sediment flux in both test conditions. Such similarities in conditions above and below the measured critical velocity highlighted the need to re-evaluate the accuracy of a single time-averaged critical velocity for the initiation of sediment entrainment.

1 Introduction

Understanding the physical processes that govern sediment resuspension has significant implications for aquatic ecosystems and fish habitats as well as sustainable engineering applications such as beach nourishment, maintenance of hydraulic structures, dam breaching flows, sedimentation in reservoirs, defence schemes against erosion due to floods, and aggregate dredging (Buffington, 1999; Paphitis, 2001; van Rijn et al., 2007; Thompson et al., 2011; Aagaard and Jensen, 2013). These necessitate improved predictive models of sediment transport. However, resuspension of sediment is a complex mechanism due to the difficulty in defining the fluctuating nature of turbulent flow. Shields (1936), the pioneer to investigate the entrainment of granular particles on a fluvial flat-bed, concluded that a critical shear stress existed below which particles did not move. At lower velocities, this critical shear stress represented the viscous drag imparted by the moving fluid to the bed particles, which is related to a critical velocity. According to this criterion (commonly used via a Shields diagram, e.g.,

Earth Surf. Dynam. Discuss., doi:10.5194/esurf-2016-60, 2016
Manuscript under review for journal Earth Surf. Dynam.
Published: 8 December 2016

Kennedy, 1995; Buffington, 1999), the critical shear stress varies as a function of the boundary Reynolds number, defined in terms of critical velocity and the particle diameter. Such approach states that sediment is entrained once bed shear stress exceeds a critical value. The Shields diagram has been extensively applied and investigated by numerous researchers (Brownlie, 1981; van Rijn, 1984; Soulsby and Whitehouse, 1997; Wu and Wang, 1999; Paphitis, 2001). However, most of those investigations were empirical with limited general applicability. Although many studies into the fluctuating nature of turbulent flow have been conducted, none of them have been able to explain turbulent effects satisfactorily (Mantz, 1977; Miller et al., 1977; Buffington, 1999; Johnson, 2016). Since earlier developed diagrams poorly fulfilled the experimental data plots in the smooth and rough-flow regimes (Yalin and Karahan, 1979), further attempts, conducting additional experiments and analysing the problem theoretically based on deterministic and probabilistic approaches, have been made to amend the Shields diagram to account for turbulent effects (Dey, 2011).

Much literature about incipient sediment motion has been published based on the concept of critical bed shear stress. A large number of researchers advocated the lift force concept, mentioning that sediment entrainment solely depended on fluid lifting force, and nearbed sediment experience lift due to the instantaneous nearbed vertical velocity, which leaded the particles to entrain (Einstein, 1950; Velikanov, 1955; Yalin, 1963; Ling, 1995). Lavelle and Mofjeld (1987) studied historical data for incipient sediment motion and found that all threshold values corresponded to a condition under which bedload transport occurred, suggesting that the critical shear stress should not be included as an essential parameter when calculating bedload transport rates. Paintal (1971) observed that there was no distinct shear stress below which no single grain entrained. Laursen et al. (1999) found that an equal-sized sediment particle had many values of the critical shear stress, which was equivalent to the number of sediment transport formulas available. The critical bed shear stress can also be excluded when computing the bedload grain velocity (Cheng and Emadzadeh, 2014).

1.1 Turbulent bursting

Kline et al. (1967) found a cyclic process with turbulent flow near walls, in which the near-wall layer propagated slowly and then interacted strongly with the outer layer flow—an event known as 'turbulent bursting'. At the beginning, the low-speed streak ejected away from the wall, and oscillations in both the spanwise and normal directions appeared. As the oscillations increased in amplitude to a certain extent, a breakdown (burst) occurred in the form of a violent and chaotic upward eruption of the low-speed fluid in the near-wall layer into the outer layer, termed usually as ejection. The ejection was soon followed by a sweep, in which the chaotic motion was swept away. The wall-layer streaks reappeared at different spanwise locations, and a new quiescent period began. The development of a horseshoe vortex showing the lifts, stretches, ejection, and sweep associated with velocity profiles is shown in Fig. 1. Such sequence of turbulent bursting involving ejection and sweep plays a central role in sediment entrainment (Cao et al., 1996).

This discovery of the turbulent bursting phenomenon led researchers to study the role of turbulence on particle entrainment and re-define the criterion of sediment movement (Dey, 2011). Several laboratory studies have linked coherent motions in the turbulent boundary layer with resuspension (Grass, 1974; Jackson, 1976; Sumer and Oguz, 1978; Sumer and

Earth Surf. Dynam. Discuss., doi:10.5194/esurf-2016-60, 2016
Manuscript under review for journal Earth Surf. Dynam.
Published: 8 December 2016

Deigaard, 1981). Grass (1974) filmed the resuspension process due to turbulent flow over a flat sand bed, identified the coherent flow structures in the boundary layer, and calculated the velocities of the particles advected by such motions. This directly led to the conclusive link between the observed ejection of fluid away from the boundary layer and the corresponding response of bed sediment. Their work also showed that the sweep events above the channel bed were more responsible for momentum transfer into the boundary layer than the ejection events. Jackson (1976) reasoned that the bursting mechanism contributed to resuspension because it allowed the sediments to maintain the vertical anisotropy of turbulence. Ejections caused an upward momentum flux on the particles, which exceeded the downward flux from the return flow for resuspending particles denser than the fluid. Sumer and Oguz (1978) and Sumer and Deigaard (1981) photographed intermittent, sweep-type fluid motions pushing sediment particles into the low-speed wall streaks; those particles were then subjected to upward, ejection-type fluid motions. Further studies (Kaftori et al., 1995; Nelson et al., 1995; Niño and Garcia, 1996; Cellino and Lemmin, 2004) confirmed the importance of the ejection and sweep phases in sediment resuspension and transport in fluvial environments.

Heathershaw and Thorne (1985) conducted experiments in tidal channels flowing over sandy gravels in order to study the role of turbulent structures on sediment entrainment, and showed that entrainment was correlated with the near wall instantaneous streamwise velocity, and not with the instantaneous Reynolds shear stress. Drake et al. (1988) studied gravel mobility in alluvial streams and found that most of the gravel entrainment was associated with sweep events, which occurred during a small fraction of time at any particular location of the bed. The entrainment process was thus found to be episodic: short periods of high entrainment were interspersed with long periods of weak or no entrainment. Thorne et al. (1989) observed that turbulent coherent structures were the main transporters of coarse sedimentary material. Their experiment suggested that an instantaneous increase in streamwise velocity fluctuations generated excess boundary shear stresses, which drove the transport. Soulsby et al. (1994) made simultaneous measurements of the high frequency fluctuations of concentration of sand suspended by a tidal current, and the horizontal and vertical components of the water velocity above the sandy bed of an estuary, and found that the large, upward sediment fluxes in the boundary layer were associated with ejection events. Kularatne and Pattiaratchi (2008) performed field experiment in the wave-induced flow environment of Floreat Beach, Perth, Western Australia and concluded that higher sediment movements are associated with ejections rather than sweeps. In the tidal current environment of western Yellow Sea of China, Yuan et al. (2009) conducted experiments and noticed that ejection and sweep events caused most of the observed turbulent sediment flux.

Although several studies have examined turbulent structures in highly variable hydrodynamic flow environments, the effect of turbulent coherent structures on sediment motions and resuspension thresholds has yet to be fully understood (Paphitis, 2001; Dey, 2011). The aim of this paper is to verify the existence of a critical velocity concept in terms of turbulent bursting phenomena. We performed laboratory experiments where high frequency data were recorded in fluvial conditions near the bottom boundary layer under unidirectional currents. Collected data were post-processed using Reynolds decomposition, quadrant analysis, and wavelet transform methods to clarify the turbulent characteristics and their effect on the resuspension mechanism both above and below the measured critical velocity test conditions.

Earth Surf. Dynam. Discuss., doi:10.5194/esurf-2016-60, 2016
Manuscript under review for journal Earth Surf. Dynam.
Published: 8 December 2016

2 Methodology

2.1 Laboratory set-up and experimental conditions

The experiments were conducted in a 54-m-long, 2-m-wide current flume located at the Environmental Hydraulics Institute (IH Cantabria), University of Cantabria, Santander, Spain. The flume contained an 18-m-long, 0.20-m-deep, purpose-built sand bed (Fig. 2). The sediment was well-sorted silica sand with a grain size of d_{50} = 0.31 mm. Two water depths were investigated, D = 0.16 m and 0.42 m. Mean flow speeds, ū, varied from 0.087 to 0.256 m/s, covering a range of Re_D=4.8×10^4-30.3×10^4.

The three-dimensional, instantaneous flow velocities were measured using eight Nortek Vectrino acoustic Doppler velocimeters (ADVs) with a sampling frequency of 50 Hz. The ADVs were located above the sand bed at distances of 5.5 m (at z = 5, 21, and 32 cm) and 8.5 m (at z = 5, 14, 21, 27, and 32 cm) from the beginning of the sand bed (Fig. 2). Data from the near-bed ADVs (z = 5cm) is used for the analysis in the present manuscript. The physical dimensions of the instruments determined the distance above the bed such that the sensors did not touch the flume bottom and would not be buried in the sand during the experiments. No bedforms developed during the experiments, the height of the sensors was constant for each test. The sand was flattened manually with a floor squeegee before each series of the tests (see Tinoco and Coco, 2014, 2016, for more details about the experimental set-up).

2.2 Data analysis techniques

Twenty-eight experiments, each lasting five minutes, were conducted to study the effect of turbulent bursting on the resuspension of sediment in the range of above the critical velocity (ACV) and below the critical velocity (BCV) test runs. The critical velocity (u_{cr} = 0.163 m/s) is obtained through data from Optical Backscatter Sensors (OBS) and ADVs as described in Tinoco and Coco (2014, 2016). The $\bar{u}/u_{cr}$ ratio for ACV was between 1.04 and 1.57, and for BCV was between 0.53 and 0.94. The results from two experiments ($\bar{u}/u_{cr}$= 1.23 ACV and $\bar{u}/u_{cr}$= 0.59 BCV) were chosen for detailed analysis in order to compare above and below the time-averaged critical velocity conditions. For both runs, we used data from the ADV located 5 cm above the sand bed and 5.5 m from the upstream edge. The measured critical velocity was 0.163 m/s and the measured water depth was 0.16 m. Two time series (both from ACV and BCV runs, each two-minute period) of the total twenty-eight experiments were also used for comparison in the quadrant analysis results.

In a series of open channel flow tests, Voulgaris and Trowbridge (1998) showed that ADVs could measure mean flows, Reynolds stresses, and vertical turbulent components close to the bed within one percent of the estimated true values. Time series records of the ADVs' high frequency (50 Hz) velocity components (where u = horizontal flow velocity, v = transverse flow velocity, and w = vertical flow velocity) were analysed using Reynolds decomposition (Fox et al., 2004), such that the flow was assumed to be composed of mean (overbar) and fluctuating (prime) parts:

$$u = \bar{u} + u', \qquad v = \bar{v} + v', \qquad w = \bar{w} + w'. \tag{1}$$

Earth Surf. Dynam. Discuss., doi:10.5194/esurf-2016-60, 2016
Manuscript under review for journal Earth Surf. Dynam.
Published: 8 December 2016

The 50 Hz time series made it difficult to distinguish clear trends; thus a one-second mean was used. To comprehend the characteristics of the bursting events, the conditional statistics of the velocity fluctuations (u′ and w′) were plotted into the quadrant on a u′-w′ plane (Lu and Willmarth, 1973), where u′ is the turbulent velocity's horizontal component and w′ is the vertical component. Quadrants were named as ejection (u′<0, w′>0), sweep (u′>0, w′<0), up-acceleration (u′>0, w′>0), and down-deceleration (u′<0, w′<0) (Heathershaw and Thorne, 1985; Kularatne and Pattiaratchi, 2008; Thorne, 2014; Schmeeckle, 2015).

Turbulent kinetic energy (TKE) shear stress was estimated using the three components of turbulent velocity (u′, v′, and w′) at the inertial subrange:

$$\tau_{TKE} = 0.5\rho C_1(u'^2 + v'^2 + w'^2), \quad (2)$$

where τ_{TKE} is the TKE shear stress, ρ is the fluid density, and C_1 is a coefficient, which can be taken as 0.19 or 0.2 (Kim et al., 2000; Biron et al., 2004). In this analysis, C_1=0.19 was used to calculate the TKE shear stress.

The turbulent Reynolds stress was estimated as (Fox et al., 2004; Thorne, 2014):

$$\tau_{Re} = -\rho(u'w'). \quad (3)$$

ADVs backscatter reading was used as a representation of suspended sediment concentration (SSC) based on the following equation (Fugate and Friedrichs, 2002; Voulgaris and Meyers, 2004):

$$EL = 0.43Amp + 20log_{10}(R) + 2\alpha_w R + 20R\int \alpha_p dr, \quad (4)$$

where EL is the echo level in dB, Amp is the amplitude in counts recorded by the ADV, R=0.05 is the range or distance between the transducer and focal point in meter, α_w=0.6 (when salinity = 0 ppt for 1.5 MHz frequency, chosen from list of values provided in Lohrmann, 2001), is the water absorption in dBm^{-1}, and α_p is the particle attenuation in dBm^{-1} (Lohrmann, 2001). At low concentrations, the particle attenuation becomes very small (Lohrmann, 2001), therefore the fourth term (i.e. $20R\int \alpha_w dr$) was ignored in this study. Additionally, to better interpret the backscatter reading as a proxy of SSC, the signal processing digital 'Butterworth' filter was used as described in Thomson and Emery (2014). Since higher SSC produces higher backscatter amplitudes, EL is used to identify instantaneous increases of SSC resulting from sweeps and ejections. We used a concentration proxy (c') as an indicator to identify variations in concentration of sediment in suspension which was also analysed using Reynolds decomposition (Fox et al., 2004), where the concentration proxy was assumed to be composed of mean (overbar) and fluctuating (prime) parts:

$$c' = EL - \overline{EL} \quad (5)$$

Wavelet analysis was used to identify localised variations of power within the time series (Torrence and Compo, 1998). The recorded time series were decomposed into time-frame space, and the dominant modes of variability and their variation in time were analysed as described in Grinsted et al. (2004). To limit the edge effects, the time series represented the region of spectrum where the effects might have been important (near large scales) by a 'Cone Of Influence (COI)' following Torrence and Compo (1998). Farge (1992) suggested that Continuous Wavelet Transform (CWT) unfolds the dynamics of coherent structures and measures their contribution to energy spectrum. Therefore, CWT was employed to derive the time evolution of momentum and sediment flux of turbulent coherent structures near the bottom boundary layer. Wavelet Coherence

Earth Surf. Dynam. Discuss., doi:10.5194/esurf-2016-60, 2016
Manuscript under review for journal Earth Surf. Dynam.
Published: 8 December 2016

(WTC) was also applied in order to expose regions with high common power showing phase relationships between the CWT of momentum and sediment flux.

3 Results

The scatterplots of the Reynolds and TKE bottom shear stresses for the ACV and BCV runs (Figs. 3a and 3b) showed that sufficient shear stress was produced to generate sediment resuspension (as shown with backscatter intensity on Figs. 4c and 5c). Such comparison of the TKE and Re shear stress methods also suggested the presence of coherent flow structures in the turbulent flow which created highly localised and persistent variability near the bed in the flow, hence affecting the bed shear stress.

The velocity fluctuations (u′, w′), Reynolds shear stress (u′w′) and backscatter over a two-minute period (for better visualisation of bursting events) from the ACV and BCV runs were compared identifying ejection and sweep events (Fig. 4, 5, respectively). This comparison offered considerable insight into the contribution of turbulence in terms of the events associated with sediment resuspension. Overall, in the time series significant variability and intermittency both in Reynolds stress (u′w′) and sediment resuspension (backscatter) was also revealed. Such intermittent nature of u′w′ was expected and observed previously in the laboratory (Grass, 1974; Jackson, 1976; Sumer and Oguz, 1978; Sumer and Deigaard, 1981; Niño et al., 2003; Schmeeckle, 2015) and in the field (Heathershaw and Thorne, 1985; Drake et al., 1988; Soulsby et al., 1994; Kularatne and Pattiaratchi, 2008 and Yuan et al., 2009). In more detail, the time series of the ACV run showed twenty-eight major resuspension events (Fig. 4). Eighteen of these events demonstrated ejections (at 5, 9, 17, 24, 30, 38, 49, 54, 66, 77, 83, 86, 98, 99, 101, 107, 109 and 116s) and ten of these events revealed sweeps (at 21, 24, 32, 42, 46, 53, 58, 61, 75 and 90s), which confirmed that high resuspension events were mostly associated with ejection and sweep type motions than up-acceleration and down-deceleration events during the analysed record. The same pattern was observed for the two-minute period of BCV run where twenty-five major resuspension events were observed (Fig. 5). Fifteen of these events were identified as ejections (at 2, 7, 19, 26, 38, 47, 52, 72, 77, 87, 90, 93, 100, 113 and 116s) and ten of these events confirmed sweeps (at 1, 32, 41, 46, 54, 60, 67, 79, 107 and 112s). Such resuspension events identified below the calculated critical velocity support the theory of the non-existence of a unique time-averaged critical shear stress as suggested by Paintal (1971) and, Lavelle and Mofjeld (1987). The plot of BCV run further indicated that though flow conditions were below the critical velocity conditions; sediment resuspension was observed due to ejection and sweep events.

Contributions to u′w′ were also observed in four quadrants of the u′-w′ plane with a threshold value (backscatter above 10 dB) both for ACV and BCV runs (Figs. 6). The plots clearly showed that the large contribution of u′ and w′ were associated with ejections and sweeps rather than up-acceleration and down-deceleration events. ACV results were similar with previous studies (Cellino and Lemmin, 2004; Yuan et al., 2009). The distribution of turbulent components for BCV in the u′-w′ plane reflected similar pattern which established that resuspension events can occur even below a critical threshold value. BCV conditions, where mean velocity was 59% of the critical velocity, showed a similar behavior to ACV conditions. Similarities

Earth Surf. Dynam. Discuss., doi:10.5194/esurf-2016-60, 2016
Manuscript under review for journal Earth Surf. Dynam.
Published: 8 December 2016

were also found in other data sets within the range of $\overline{u}/u_{cr}$ ratio; for ACV between 1.04 and 1.57, and for BCV between 0.53 and 0.94.

We performed a quadrant analysis to determine the frequency of different bursting events and their contributions to the Reynolds stress (i.e. u′w′). The occurrence percentages of four types of bursting motions, as well as their contributions to the momentum flux (u′w′) and sediment flux (c′w′) for the ACV and BCV experiments, are shown in Figs. 7 and 8, respectively. The results for the u′w′ signals for the ACV and BCV experiments agreed with the results from earlier studies (Wallace et al., 1972; Willmarth and Lu, 1972). For both ACV and BCV experiments, ejection and sweep events were the dominant source of the Reynolds stress; however, although the time occupied by ejection was comparable with, or even less than, that of sweep, ejection contributed more to the net Reynolds stress (ACV = 49%; BCV = 43%) as shown in Figs. 7a,b and 8a,b. Ejection (ACV = 38%; BCV = 38%) and sweep (ACV = 37%, BCV = 30%) mainly generated the upward sediment flux (Figs. 7c and 8c), which suggested the intense upwelling of low-speed fluid parcels with high sediment entrainment events was the main source of the overall sediment flux. In contrast, up-acceleration (ACV = 12%; BCV = 14%) and down-deceleration (ACV = 13%; BCV = 18%) events transported less sediment (Figs. 7c and 8c). Thus ejection and sweep contributed more to the total turbulent sediment flux (ACV = 75%; BCV = 68%) than up-acceleration and down-deceleration events (ACV = 25%; BCV = 32%). Such consistent results in both ACV and BCV confirm the need to develop transport rate formulas that consider instantaneous Reynolds stress concepts along time-averaged critical velocities.

Continuous Wavelet Transforms (CWT) and Wavelet Coherence (WTC) analysis (Grinsted et al., 2004) for ACV and BCV runs offered a more intuitive way to visualise the turbulence data in both time and space (Figs. 9 and 10, respectively). In the presented scalograms, warmer colours indicated higher energy. It is noteworthy to mention that, at higher periods (i.e. low frequency events), the power felt within the range of COI (i.e. the shaded region in the scalograms) which limited the capability to investigate the temporal evolution of the specific peak frequencies as stated in Section 2.2. Hence, investigation was restricted to examine high frequency events occurring at time scales up to 32s for both runs. Overall, the scalograms (Figs. 9 and 10) traced the dynamics of coherent structures and its measured contribution to the sediment flux. It also revealed that within the large-scale motions, there existed multi-scale and some embedding small fine-scale features. This suggested that both for ACV and BCV runs, near the bed, most of the energy was concentrated within the high period associated with the mean flow properties for both momentum flux and sediment flux. Results also showed that highly energy turbulent events occurred i) sporadically throughout the time series, especially in gradually developing clusters that sustained short periods in the dominant direction of flow near the bed, ii) for longer periods (up to several seconds from a turbulence perception), vertically in the water column, and iii) at lower frequencies for both runs. The larger clusters felt over 1 and 8s period band for both ACV and BCV runs; while the fast evolving clusters stretched between 0.0625 and 0.5s period band before weakening. This was evident in the colour coded contours (Fig. 9a) which were associated with ejection (at 5, 9, 17, 24, 30, 38, 49, 54, 66, 77, 83, 86, 98, 99, 101, 107, 109 and 116s) and sweep (at 21, 24, 32, 42, 46, 53, 58, 61, 75 and 90s) events for ACV runs. Similarly, for BCV runs; it was evident with ejection (at 2, 7, 19, 26, 38, 47, 52, 72, 77, 87, 90, 93, 100, 113 and 116s) and

Earth Surf. Dynam. Discuss., doi:10.5194/esurf-2016-60, 2016
Manuscript under review for journal Earth Surf. Dynam.
Published: 8 December 2016

sweep (at 1, 32, 41, 46, 54, 60, 67, 79, 107 and 112s) events. In addition to that, in ACV runs; momentum flux corresponded to the contour in sediment flux within similar period bands both in ejection (at 5, 9, 17, 24, 30, 38, 49, 54, 66, 77, 83, 86, 98, 99, 101, 107, 109 and 116s) and sweep (at 21, 24, 32, 42, 46, 53, 58, 61, 75 and 90s) events as shown in Figs. 9a and b. Similar pattern was also observed in BCV runs at 2, 7, 19, 26, 38, 47, 52, 72, 77, 87, 90, 93, 100, 113 and 116s (ejection events), as well as at 1, 32, 41, 46, 54, 60, 67, 79, 107 and 112s (sweep events) where momentum and sediment flux coincide with each other showing similar period bands (Figs. 10a and b). The WTC was applied to the momentum and sediment flux for both runs where common features were noticed as shown in Figs. 9c and 10c. Both for ACV and BCV runs, at high period bands the coherence were found to be higher compared to lower period bands, suggesting that the transport mechanism greatly relies on the production of momentum flux by coherent structures in order to contribute to the sediment flux.

4 Discussion

Comparison of test results where mean velocity was 1.23 times higher as well as 0.59 times lower the measured critical velocity showed strong similarities without major exceptions (Figs. 4 and 5). Although nearbed velocity and average transport rate were greater in ACV runs, the peak instantaneous transport rates were close in both cases (i.e. ACV and BCV runs). Both ejection and sweep events contributed to the forward momentum flux as well as sediment flux which highlighted that the concept of time-averaged critical velocity by itself cannot provide a full representation of the physical processes active in the resuspension of sediment.

In both tests (ACV and BCV), ejection and sweep events were the largest contributors to momentum transfer. Up-acceleration and down-deceleration events lead to marginal effect on transport of momentum and sediment flux compared to the other two events (Fig. 6). Although Heathershaw and Thorne (1985) advised that up-acceleration and down-deceleration events considerably contributed to resuspend sediment, reasonably less net sediment flux was accomplished by these events in our ACV and BCV runs. These could be related to the strength of the up-acceleration and down-deceleration events which were much weaker and could not carry sediment particles to a higher level where the sampling volume was placed (i.e., 5 cm above the bed). It is also noteworthy to mention that up-acceleration and down-deceleration events contributed less significantly with a positive stress. Quadrant analysis showed that, in BCV runs, ejection (in which low speed fluid moves away from the boundary towards the outer layer) entrained particles away from the bed in order to maintain them in suspension as it was in ACV runs (Figs. 7 and 8). Sweeps, (in which high-speed fluid moves near the wall) with a negative contribution, impacted on the particles in resuspension by pushing them towards the bed. Moreover, the time occupied in both ACV and BCV runs were almost identical and contributed in similar percentage to instantaneous momentum and sediment flux as well.

Wavelet analysis was useful to diagnose characteristics of turbulence in order to explain information about the spatial structure of the flow. Particularly, we were interested in its frequency content and energy variation (Figs. 9 and 10). Measured data in BCV runs were consistent with ACV runs. The scalograms, which presented the time series records for both ACV and BCV runs, showed the presence of both multi-scale and small-fine scale features within large-scale motions. The cross wavelet

Earth Surf. Dynam. Discuss., doi:10.5194/esurf-2016-60, 2016
Manuscript under review for journal Earth Surf. Dynam.
Published: 8 December 2016

transform method was effective at visualising and detecting the coherent structures from the raw turbulent data, which enabled us to study the correlation between wall turbulence structures and sediment resuspension.

5 Conclusions

We examined the influence of turbulent coherent structures on resuspending sediment for flows both above and below the critical resuspension velocity. Results showed that the measured critical velocity alone was not sufficient to predict episodic initiation of motion, as turbulent events can move sediment even at mean flow conditions below the thresholds defined by time-averaged stresses. Measured fluctuations of turbulent Reynolds stress evidenced to move sediments at lower turbulent stresses than expected. Instantaneous particle entrainment occurred earlier than the suggested measured time-averaged critical velocity due to the stochastic nature of turbulence. Although nearbed shear stress can be used to estimate bedload transport, significant special variations in the magnitudes and durations of the ejection, sweep, up-acceleration and down-deceleration plays a significant role in sediment resuspension. The implications of sediment motion at Reynolds shear stress below the expected critical conditions further suggested that instantaneous shear stress has an important contribution to entrain particles, which cannot be predicted with a time averaged critical velocity.

To the best of our knowledge, there is no universal agreement on identifying a unique threshold for initiation of motion or resuspension of sediment (e.g., how many grains rolling, for how long, over what area coverage) in the literature. Our study shows that turbulent bursting events produce sediment resuspension even at mean velocities well below such typical critical values. Our statistical assessment suggests that the existing definition of threshold can be improved by incorporating turbulent effects for a more accurate description of the processes involved which will result in better predictions of sediment transport.

Acknowledgement

This work was a part of the first author's PhD research when he was in receipt of Scholarship for International Research Fees (SIRF), University International Stipend (UIS) and Safety Net Top-Up Scholarship awarded by the UWA Oceans Institute and the School of Civil Environmental and Mining Engineering at the University of Western Australia, Australia. Authors gratefully acknowledge the support of the Environmental Hydraulics Institute (IH Cantabria), University of Cantabria, Spain providing the data. GC funded by the Natural Hazards Research Platform (C05X0907). In addition to that, authors would like to express their appreciation to Dr Florence Verspecht and Ruth Gongora-Mesas for their assistance in preparing the final manuscript.

Earth Surf. Dynam. Discuss., doi:10.5194/esurf-2016-60, 2016
Manuscript under review for journal Earth Surf. Dynam.
Published: 8 December 2016

References

Aagaard, T., and Jensen, S. G.: Sediment concentration and vertical mixing under breaking waves, Marine Geology, 336, 146-159, doi.org/10.1016/j.margeo.2012.11.015, 2013.

Biron, P. M., Robson, C., Lapointe, M. F., and Gaskin, S. J.: Comparing different methods of bed shear stress estimates in simple and complex flow fields, Earth Surf. Process. Landf., 29, 1403-1415, doi:10.1002/esp.1111, 2004.

Brownlie, W. R.: Prediction of flow depth and sediment discharge in open channels, Ph.D. Thesis, Engineering and Applied Science, California Institute of Technology, California, 1981.

Buffington, J. M.: The Legend of A. F. Shields, J. Hydraul. Eng., 125, 376-387, doi:10.1061/(ASCE)0733-9429(1999)125:4(376), 1999.

Buffington, J. M., and Montgomery, D. R.: Effects of sediment supply on surface textures of gravel-bed rivers, Water Resour. Res., 35, 3523-3530, doi:10.1029/1999wr900232, 1999.

Cao, Z., Xi, H., and Zhang, X.: Turbulent bursting-based diffusion model for suspended sediment in open channel flows, J. Hydraul Res, 34, 457-472, doi:10.1080/00221689609498471, 1996.

Cellino, M., and Lemmin, U.: Influence of Coherent Flow Structures on the Dynamics of Suspended Sediment Transport in Open-Channel Flow, J. Hydraul. Eng., 130, 1077-1088, doi:10.1061/(ASCE)0733-9429(2004)130:11(1077), 2004.

Cheng, N., and Emadzadeh, A.: Average Velocity of Solitary Coarse Grain in Flows over Smooth and Rough Beds, J. Hydraul. Eng., 140, 04014015, doi:10.1061/(ASCE)HY.1943-7900.0000875, 2014.

Dey, S.: Entrainment Threshold of Loose Boundary Streams, in: Experimental Methods in Hydraulic Research, edited by: Rowinski, P., Springer Berlin Heidelberg, Berlin, Heidelberg, 29-48, 2011.

Drake, T. G., Shreve, R. L., Dietrich, W. E., Whiting, P. J., and Leopold, L. B.: Bedload transport of fine gravel observed by motion-picture photography, J. Fluid Mech., 192, 193-217, doi:10.1017/S0022112088001831, 1988.

Einstein, H.A.: The bed-load function for sediment transportation in open channel flows. US Department of Agriculture, Washington DC, Technical bulletin number 1026, 1950.

Farge, M.: Wavelet Transforms and their Applications to Turbulence, Ann. Rev. Fluid Mech., 24, 395-458, doi:10.1146/annurev.fl.24.010192.002143, 1992.

Fox, R. W., McDonald, A. T., and Pritchard, P. J.: Introduction to fluid mechanics, 6th ed., Wiley and Sons, USA, 2004.

Fugate, D. C., and Friedrichs, C. T.: Determining concentration and fall velocity of estuarine particle populations using ADV, OBS and LISST, Cont. Shelf Res., 22, 1867-1886, doi.org/10.1016/S0278-4343(02)00043-2, 2002.

Grass, A. J.: Transport of fine sand on a flat bed: turbulence and suspension mechanics. In: Transport, Erosion and Deposition of Sediment in Turbulent Streams, Proc. Euromech, 1974.

Grinsted, A., Moore, J. C., and Jevrejeva, S.: Application of the cross wavelet transform and wavelet coherence to geophysical time series, Nonlin. Processes Geophys., 11, 561-566, doi:10.5194/npg-11-561-2004, 2004.

Heathershaw, A. D., and Thorne, P. D.: Seabed noises reveal role of turbulent bursting phenomenon in sediment transport by tidal currents, Nature, 316, 339-342, 1985.

Jackson, R. G.: Sedimentological and fluid-dynamic implications of the turbulent bursting phenomenon in geophysical flows, J. Fluid Mech., 77, 531-560, doi:10.1017/S0022112076002243, 1976.

Johnson, J. P. L.: Gravel threshold of motion: a state function of sediment transport disequilibrium?, Earth Surf. Dynam., 4, 685-703, doi:10.5194/esurf-4-685-2016, 2016.

Kaftori, D., Hetsroni, G., and Banerjee, S.: Particle behavior in the turbulent boundary layer. I. Motion, deposition, and entrainment, Physics of Fluids, 7, 1095-1106, doi:org/10.1063/1.868551, 1995.

Kennedy, J. F.: The Albert Shields Story, J. Hydraul. Eng., 121, 766-772, doi:10.1061/(ASCE)0733-9429(1995)121:11(766), 1995.

Kim, S., Friedrichs, C., Maa, J., and Wright, L.: Estimating Bottom Stress in Tidal Boundary Layer from Acoustic Doppler Velocimeter Data, J. Hydraul. Eng., 126, 399-406, doi:10.1061/(ASCE)0733-9429(2000)126:6(399), 2000.

Kline, S. J., Reynolds, W. C., Schraub, F. A., and Runstadler, P. W.: The structure of turbulent boundary layers, J. Fluid Mech., 30, 741-773, doi:10.1017/S0022112067001740, 1967.

Kolmogorov, A. N.: The local structure of turbulence in incompressible viscous fluids at very large Reynolds numbers, Dokl Akad Nauk SSSR, 30, 299-303, 1941.

Kularatne, S., and Pattiaratchi, C.: Turbulent kinetic energy and sediment resuspension due to wave groups, Cont. Shelf Res., 28, 726-736, doi:10.1016/j.csr.2007.12.007, 2008.

Laursen, E., Papanicolaou, A., Cheng, N., and Chiew, Y.: Discussions and Closure: Pickup Probability for Sediment Entrainment, J. Hydraul. Eng., 125, 786-789, doi:10.1061/(ASCE)0733-9429(1999)125:7(789.x), 1999.

Lavelle, J., and Mofjeld, H.: Do Critical Stresses for Incipient Motion and Erosion Really Exist?, J. Hydraul. Eng., 113, 370-385, doi:10.1061/(ASCE)0733-9429(1987)113:3(370), 1987.

Li, X., Zimmerman, N., and Princevac, M.: Characterization of Turbulent Kinetic Energy budges in the atmospheric surface layer, 16th Conference on Atmos. Ocean. Fluid Dynamics, 2007.

Ling, C.H.: Criteria for incipient motion of spherical sediment particles. J. Hydraul. Eng., 121, 472–478, 1995.
Lohrmann, A.: Monitoring Sediment Concentration with acoustic backscattering instruments, Nortek Tehcnical Note No. 003, 1-5, 2001.
Lu, S. S., and Willmarth, W. W.: Measurements of the structure of the Reynolds stress in a turbulent boundary layer, J. Fluid Mech., 60, 481-511, doi:10.1017/S0022112073000315, 1973.
Mantz, P. A.: Incipient transport of fine grains and flanks by fluids-extended Shields diagram, J. Hydraul. Div., 130, 601–615, 1977.
Miller, M. C., McCave, I. N., and Komar, P. D.: Threshold of sediment motion under unidirectional currents, Sedimentology, 24, 507-527, doi:10.1111/j.1365-3091.1977.tb00136.x, 1977.
Nelson, J. M., Shreve, R. L., McLean, S. R., and Drake, T. G.: Role of Near-Bed Turbulence Structure in Bed Load Transport and Bed Form Mechanics, Water Resour. Res., 31, 2071-2086, doi:10.1029/95WR00976, 1995.
Niño, Y., Lopez, F., and Garcia, M.: Threshold for particle entrainment into suspension, Sedimentology, 50, 247-263, doi:10.1046/j.1365-3091.2003.00551.x, 2003.
Niño, Y., and Garcia, M. H.: Experiments on particle—turbulence interactions in the near–wall region of an open channel flow: implications for sediment transport, J. Fluid Mech., 326, 285-319, doi:10.1017/S0022112096008324, 1996.
Paintal, A. S.: Concept Of Critical Shear Stress In Loose Boundary Open Channels, J. Hydraul. Res., 9, 91-113, doi:10.1080/00221687109500339, 1971.
Paphitis, D.: Sediment movement under unidirectional flows: an assessment of empirical threshold curves, Coastal Eng., 43, 227-245, doi:10.1016/s0378-3839(01)00015-1, 2001.
Schmeeckle, M. W.: The role of velocity, pressure, and bed stress fluctuations in bed load transport over bed forms: numerical simulation downstream of a backward-facing step, Earth Surf. Dynam., 3, 105-112, doi:10.5194/esurf-3-105-2015, 2015.
Shields, A. F.: Application of similarity principles and turbulence research to bed-load movement, Mitteilungen der Preussischen Versuchsanstalt f€ur Wasserbau und Schiffbau, Berlin, Germany, Berlin, Germany, 5-24, 1936.
Soulsby, R. L., Atkins, R., and Salkield, A. P.: Observations of the turbulent structure of a suspension of sand in a tidal current, Cont. Shelf Res., 14, 429-435, doi:10.1016/0278-4343(94)90027-2, 1994.
Soulsby, R. L., Whitehouse, R. J. S.: Threshold of sediment motion in coastal Environments. Proceedings of the Combined Australasian Coastal Engineering and Port Conference, Christchurch, 149–154. 1997
Sumer, B. M., and Oguz, B.: Particle motions near the bottom in turbulent flow in an open channel, J. Fluid Mech., 86, 109-127, doi:10.1017/S0022112078001020, 1978.
Sumer, B. M., and Deigaard, R.: Particle motions near the bottom in turbulent flow in an open channel. Part 2, J. Fluid Mech., 109, 311-337, doi:10.1017/S0022112081001092, 1981.
Thomson, R. E., and Emery, W. J.: Chapter 6 - Digital Filters, in: Data Analysis Methods in Physical Oceanography (Third Edition), Elsevier, Boston, 593-637, 2014.
Thompson, C. E. L., Couceiro, F., Fones, G. R., Helsby, R., Amos, C. L., Black, K., Parker, E. R., Greenwood, N., Statham, P. J., and Kelly-Gerreyn, B. A.: In situ flume measurements of resuspension in the North Sea, Estuar., Coast. and Shelf Sci., 94, 77-88, doi.org/10.1016/j.ecss.2011.05.026, 2011.
Thorne, P. D., Williams, J. J., and Heathershaw, A. D.: In situ acoustic measurements of marine gravel threshold and transport, Sedimentology, 36, 61-74, doi:10.1111/j.1365-3091.1989.tb00820.x, 1989.
Thorne, P. D.: An overview of underwater sound generated by interparticle collisions and its application to the measurements of coarse sediment bedload transport, Earth Surf. Dynam., 2, 531-543, doi:10.5194/esurf-2-531-2014, 2014.
Tinoco, R. O., and Coco, G.: Observations of the effect of emergent vegetation on sediment resuspension under unidirectional currents and waves, Earth Surf. Dynam., 2, 83-96, doi:10.5194/esurf-2-83-2014, 2014.
Tinoco, R. O., and Coco, G.: A laboratory study on sediment resuspension within arrays of rigid cylinders, Advances in Water Resour., 92, 1-9, doi.org/10.1016/j.advwatres.2016.04.003, 2016.
Torrence, C., and Compo, G. P.: A Practical Guide to Wavelet Analysis, Bulletin of the American Meteo. Soc., 79, 61-78, doi:10.1175/1520-0477(1998)079<0061:APGTWA>2.0.CO;2, 1998.
van Rijn, L. C.: Sediment Transport, Part I: Bed Load Transport, J. Hydraul. Eng., 110, 1431-1456, doi:10.1061/(ASCE)0733-9429(1984)110:10(1431), 1984.
van Rijn, L. C., Walstra, D.-J. R., and van Ormondt, M.: Unified View of Sediment Transport by Currents and Waves. IV: Application of Morphodynamic Model, J. Hydraul. Eng., 133, 776-793, doi:10.1061/(ASCE)0733-9429(2007)133:7(776), 2007.
Velikanov, M.A.: Dynamics of alluvial stream, 2, State Publishing House of Theoretical and Technical Literature, Russia (in Russian), 1955.
Voulgaris, G., and Trowbridge, J. H.: Evaluation of the acoustic Doppler velocimeter (ADV) for turbulence measurements, J. Atmos. Ocean. Tech., 15, 272-289, doi:10.1175/1520-0426(1998)015<0272:eotadv>2.0.co;2, 1998.
Voulgaris, G., and Meyers, S. T.: Temporal variability of hydrodynamics, sediment concentration and sediment settling velocity in a tidal creek, Cont. Shelf Res., 24, 1659-1683, doi:org/10.1016/j.csr.2004.05.006, 2004.

Earth Surf. Dynam. Discuss., doi:10.5194/esurf-2016-60, 2016
Manuscript under review for journal Earth Surf. Dynam.
Published: 8 December 2016

Wallace, J. M., Eckelmann, H., and Brodkey, R. S.: The wall region in turbulent shear flow, J. Fluid Mech., 54, 39-48 M33 - doi:10.1017/S0022112072000515, 1972.
Willmarth, W. W., and Lu, S. S.: Structure of the Reynolds stress near the wall, J. Fluid Mech., 55, 65-92 M63 - doi:10.1017/S002211207200165X, 1972.
Wu, W., and Wang, S. S. Y.: Movable Bed Roughness in Alluvial Rivers, J. Hydraul. Eng., 125, 1309-1312, doi:10.1061/(ASCE)0733-9429(1999)125:12(1309), 1999.
Yalin, M.S.: An expression of bed-load transportation. J. Hydraul. Div., 89, 221–250, 1963.
Yalin, M. S., and Karahan, E.: Inception of sediment transport, J. Hydraul. Div., 105, 1433-1443, 1979.
Yuan, Y., Wei, H., Zhao, L. A., and Cao, Y. N.: Implications of intermittent turbulent bursts for sediment resuspension in a coastal bottom boundary layer: A field study in the western Yellow Sea, China, Marine Geology, 263, 87-96, doi:10.1016/j.margeo.2009.03.023, 2009.

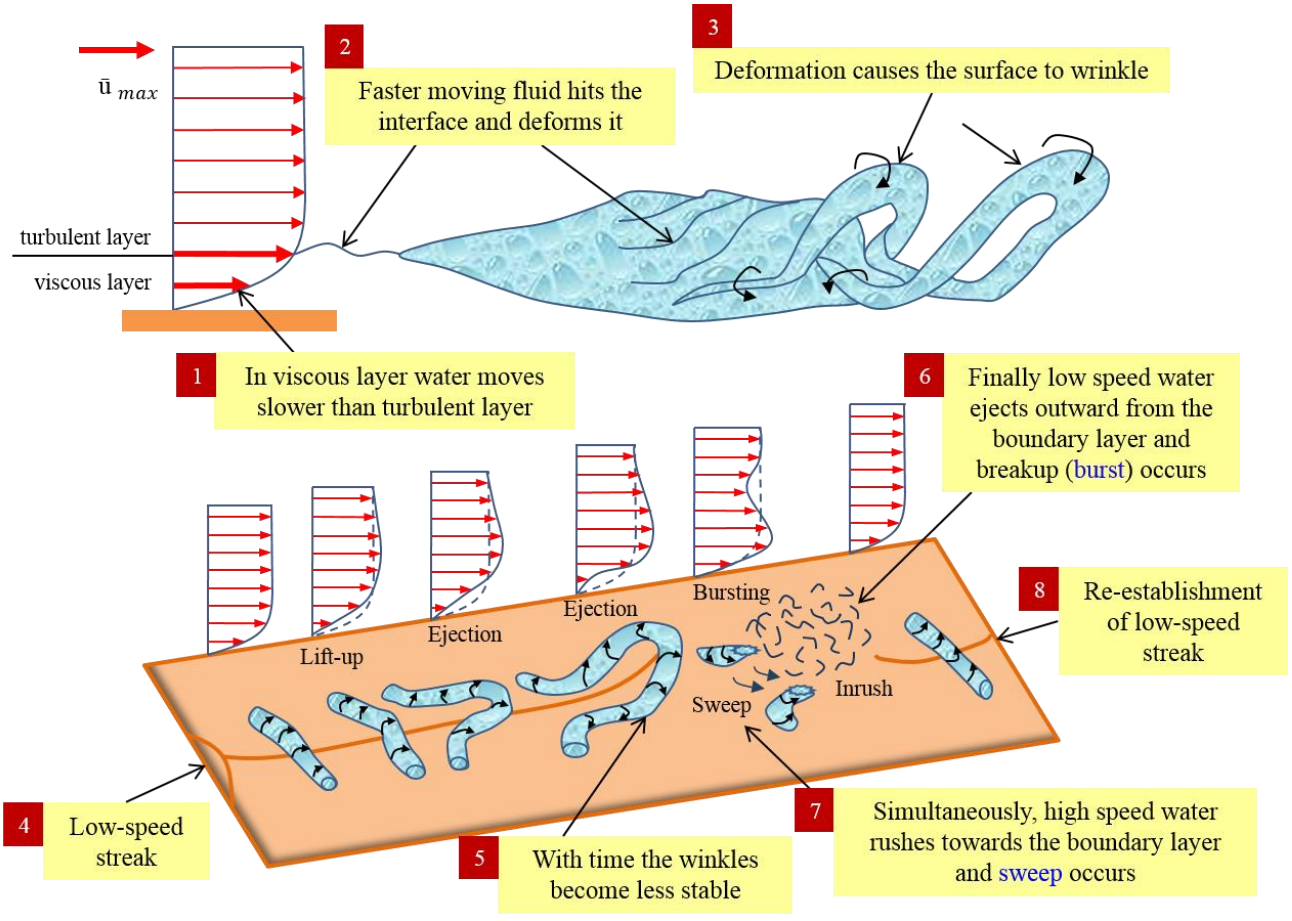

Figure 1. Schematic diagram of the typical sequence of turbulent bursting phenomena (Allen, 1985; Bridge, 2003) where the flow is directed from left to right and the arrow length represents the relative velocity in the velocity profiles.

Earth Surf. Dynam. Discuss., doi:10.5194/esurf-2016-60, 2016
Manuscript under review for journal Earth Surf. Dynam.
Published: 8 December 2016

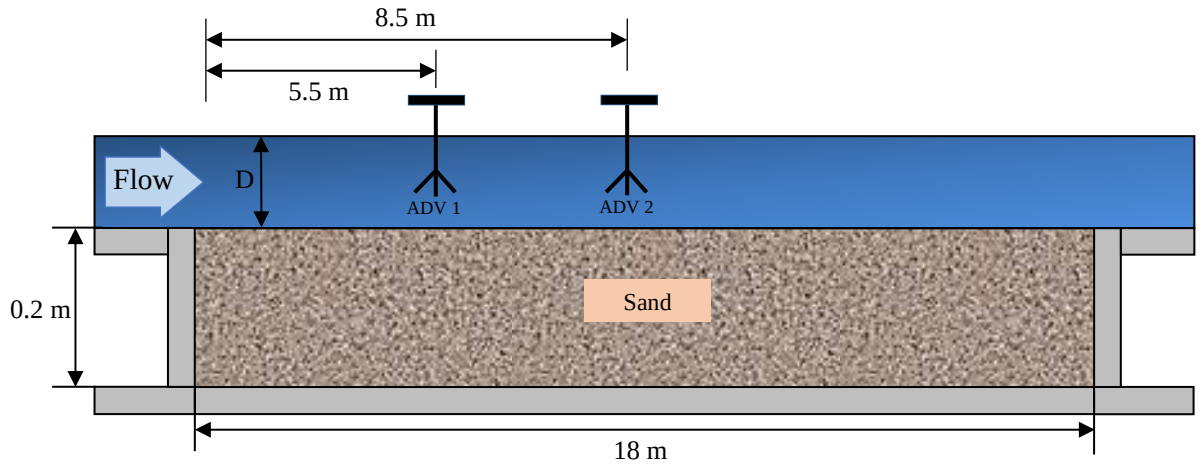

Figure 2. Schematic diagram of the experimentation flume showing the key dimensions and ADV locations.

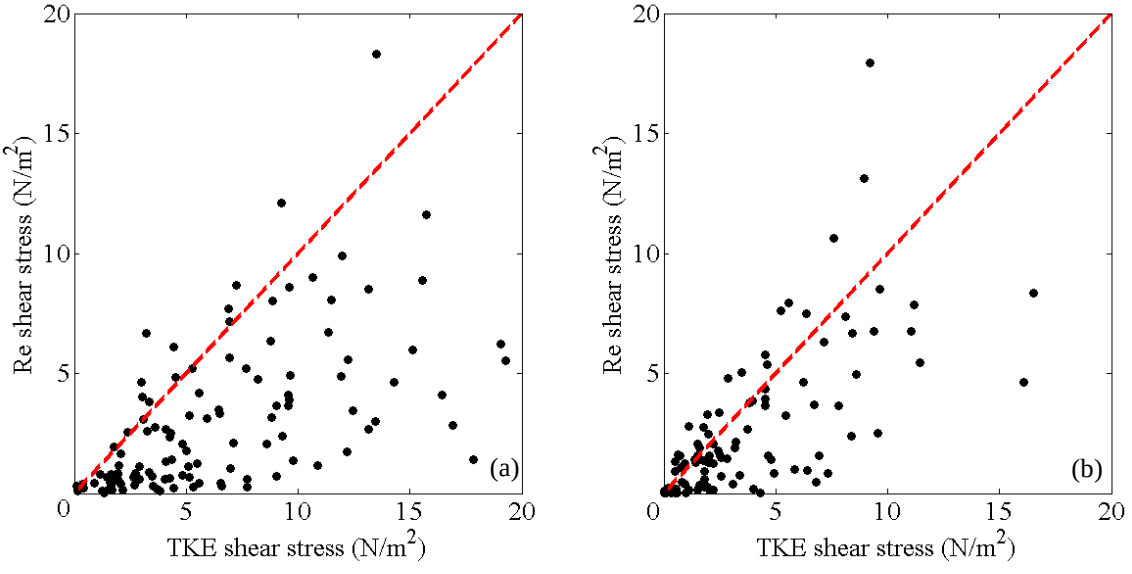

Figure 3. Comparison of the one-second mean Reynolds and TKE shear stresses from (a) above the critical velocity ($\bar{u} > u_{cr}$) and (b) below the critical velocity ($\bar{u} < u_{cr}$) experiments with a two-minute period. The dashed red line defines the equality.

Earth Surf. Dynam. Discuss., doi:10.5194/esurf-2016-60, 2016
Manuscript under review for journal Earth Surf. Dynam.
Published: 8 December 2016

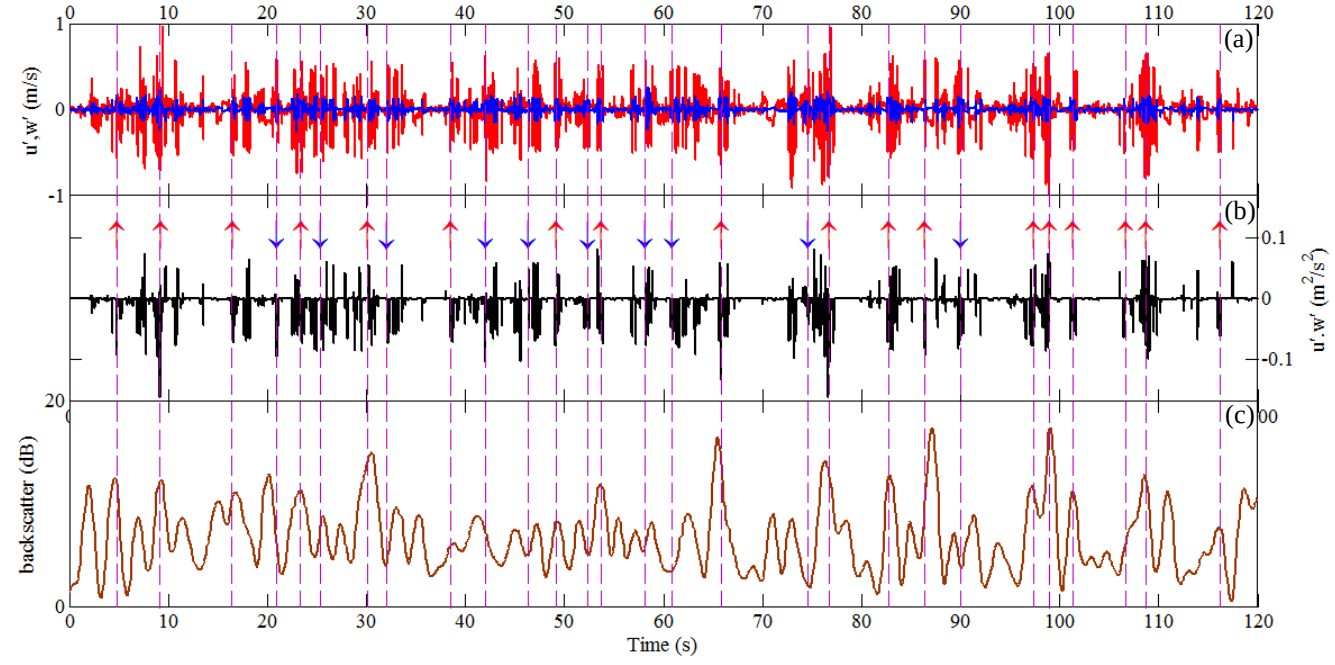

Figure 4. Time series records from the above critical velocity experiment ($\bar{u} > u_{cr}$): (a) turbulent velocity (u′ - red in color, w′ - blue in color); (b) turbulent Reynolds shear stress (u′w′), showing the ejection (red up arrows) and sweep (blue down arrows) events; (c) one-second mean of the backscatter.

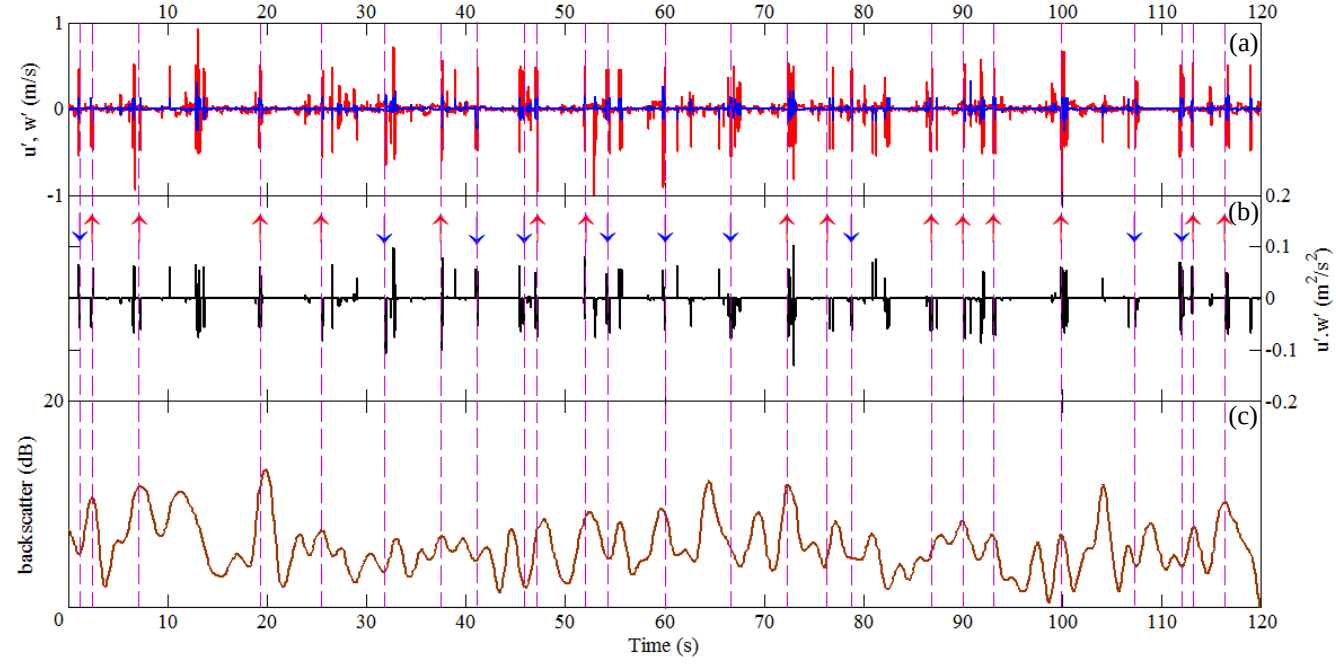

Figure 5. Time series records from below the critical velocity experiment ($\bar{u} < u_{cr}$): (a) turbulent velocity (u′, w′); (b) turbulent Reynolds shear stress (u′w′), showing the ejection (red up arrows) and sweep (blue down arrows) events; (c) one-second mean of the backscatter.

Earth Surf. Dynam. Discuss., doi:10.5194/esurf-2016-60, 2016
Manuscript under review for journal Earth Surf. Dynam.
Published: 8 December 2016

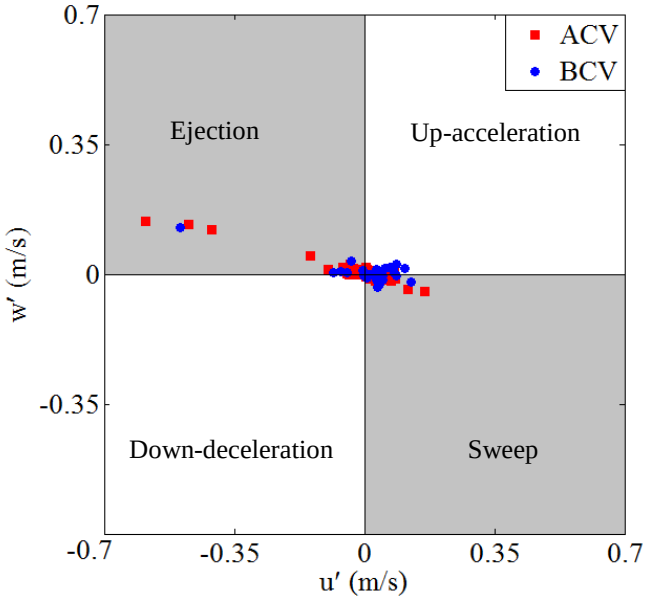

Figure 6: Classification of bursting events in u′-w′ space mentioning ejection, sweep, up-acceleration and down-deceleration events both for above and below the critical velocity conditions.

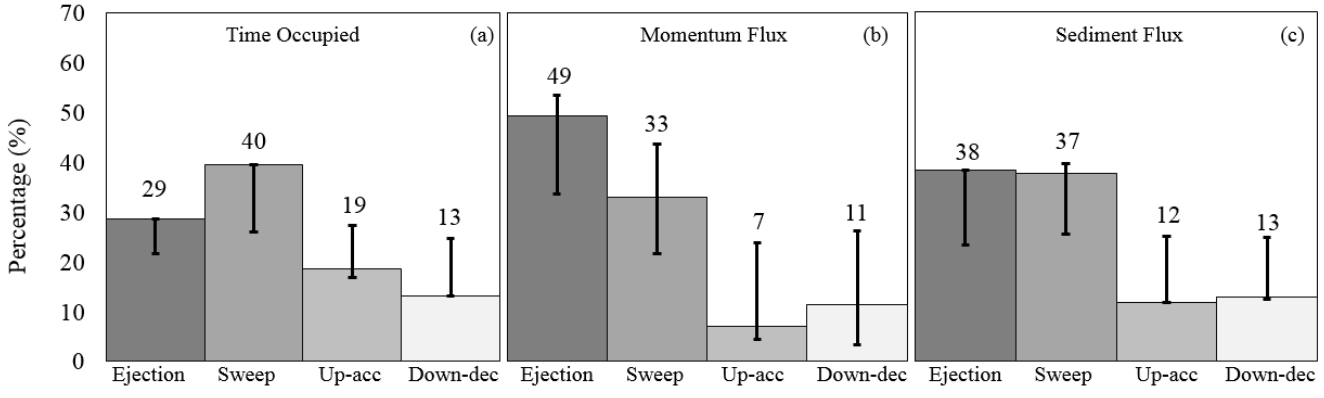

Figure 7. Quadrant analysis of coherent structures in above the critical velocity ranges ($\bar{u} > u_{cr}$) showing the (a) time occupied, (b) momentum flux (u′w′), and (c) sediment flux (c′w′). The error bars represent the maximum and minimum values of the total data.

Earth Surf. Dynam. Discuss., doi:10.5194/esurf-2016-60, 2016
Manuscript under review for journal Earth Surf. Dynam.
Published: 8 December 2016

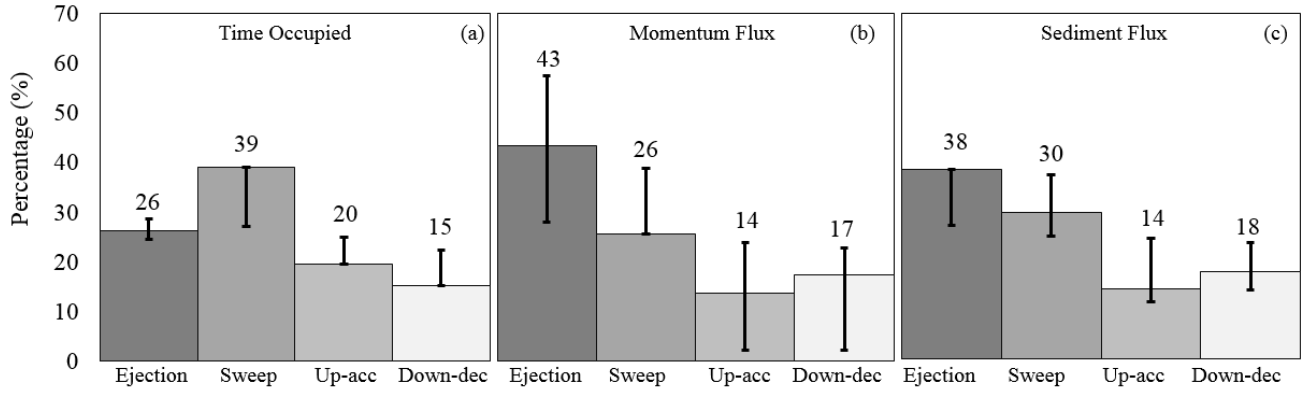

Figure 8. Quadrant analysis of coherent structures in below the critical velocity range ($\bar{u} < u_{cr}$) showing the (a) time occupied, (b) momentum flux ($u'w'$), and (c) sediment flux ($c'w'$). The error bar represents the maximum and minimum values of the total data.

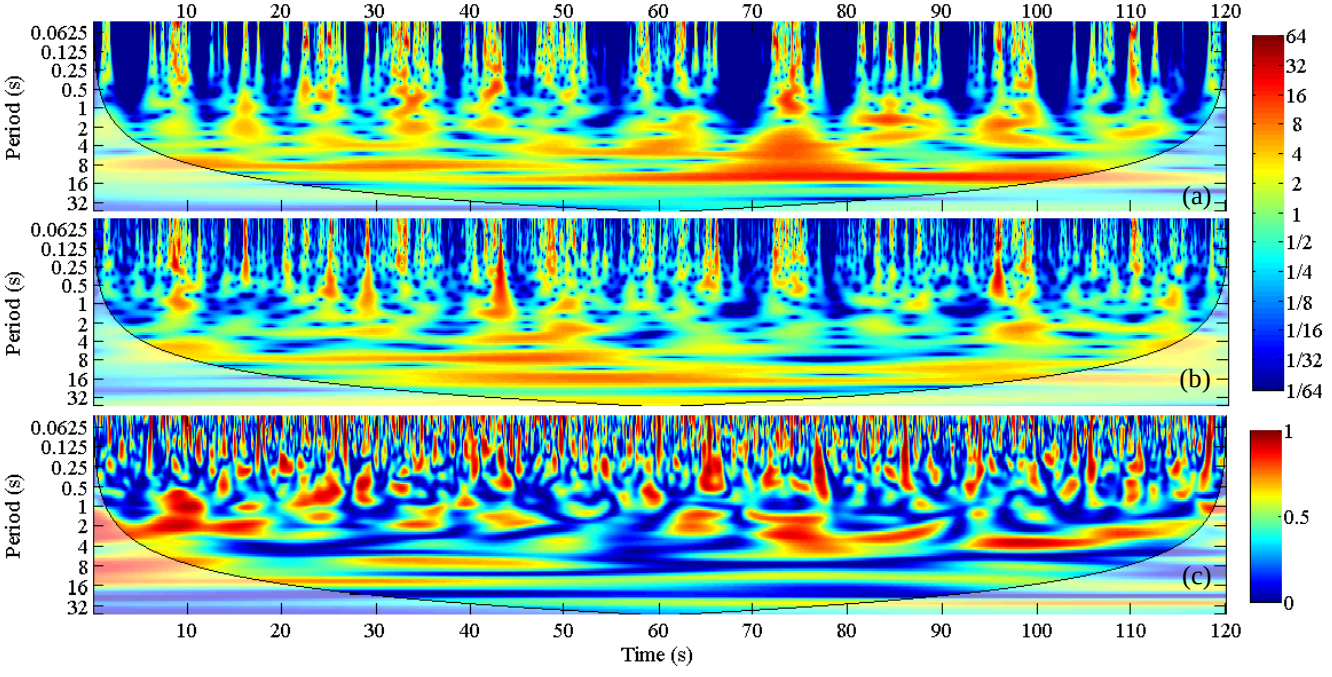

Figure 9. Wavelet power spectra (Morlet wavelet) for above the critical velocity experiment ($\bar{u} > u_{cr}$) for a two-minute period showing the (a) momentum flux ($u'w'$), (b) sediment flux ($c'w'$), and (c) coherence between the momentum and sediment fluxes.

Earth Surf. Dynam. Discuss., doi:10.5194/esurf-2016-60, 2016
Manuscript under review for journal Earth Surf. Dynam.
Published: 8 December 2016

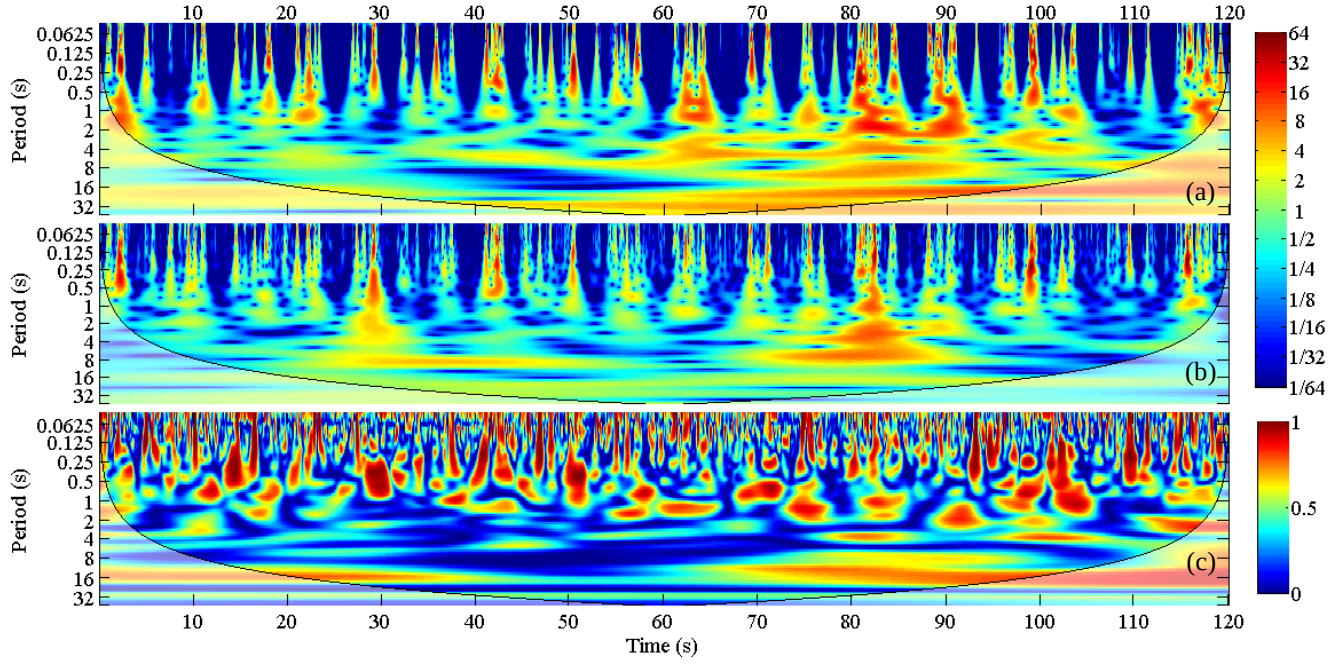

Figure 10. Wavelet power spectra (Morlet wavelet) for below the critical velocity experiment ($\bar{u} < u_{cr}$) for a two-minute period showing the (a) momentum flux (u′w′), (b) sediment flux (c′w′), and (c) coherence between the momentum and sediment fluxes.